Binding and Redox Properties of Iron(II) Bonded to an Oxo Surface Modeled by Calix[4]arene

Vittorio Esposito, Euro Solari, and Carlo Floriani*

Institut de Chimie Minérale et Analytique, BCH, Université de Lausanne, CH-1015 Lausanne, Switzerland

Nazzareno Re

Facoltà di Farmacia, Università degli Studi "G. D'Annunzio", I-66100 Chieti, Italy

Corrado Rizzoli and Angiola Chiesi-Villa

Dipartimento di Chimica, Università di Parma, I-43100 Parma, Italy

Received December 21, 1999

The syntheses of the parent compounds [{*p*-Bu^t−calix[4]−$(O)_2(OR)_2$}Fe−L] [R = Me, L = THF, **5**; R = Bu^n, L = THF, **6**; R = $PhCH_2$, L = THF, **7**; R = $SiMe_3$, L = none, **8**] have been performed by reacting the protonated form of the dialkylcalix[4]arene with [Fe_2Mes_4] [Mes = 2,4,6-$Me_3C_6H_2$]. All of them undergo one-electron oxidative functionalization. By use of different oxidizing agents, the following iron(III) derivatives have been obtained: [{*p*-Bu^t−calix[4]−$(O)_2(OR)_2$}Fe−X] [X = Cl, R = Me, **9**; X = I, R = Me, **10**] and [{*p*-Bu^t−calix[4]−$(O)_2(OR)_2$}$_2$$Fe_2$($\mu$-X] [X = O, R = Me, **11**; X = O, R = Bu^n, **12**; X = S, R = Me, **13**], **9** and **10** being particularly appropriate for a further functionalization of the metal. The last three display typical antiferromagnetic behavior [$J = -78.6$ cm^{-1}, **11**; $J = -64.1$ cm^{-1}, **13**]. In the case of **7** and **8**, the reaction with O_2 led to the dealkylation of one of the alkoxo groups, with the formation of a dimeric iron(III) derivative {[μ-*p*-Bu^t−calix[4]−$(O)_3(OR)$}$_2$$Fe_2$] [R = $PhCH_2$, **14**; R = $SiMe_3$, **15**] [$J = -9.8$ cm^{-1}]. The reaction of the parent compounds with Bu^{t}NC and diazoalkanes led to the formation of [Fe═C] functionalities supported by a calix[4]arene oxo surface. The following compounds have been isolated and characterized: {[*p*-Bu^t−calix[4]−$(O)_2(OR)_2$}Fe═CNBu^t] [R = $SiMe_3$, **16**, $\nu_{CN} = 2175$ cm^{-1}], {[*p*-Bu^t−calix[4]−$(O)_2(OR)_2$}Fe═CPh_2] [R = Me, **17**; R = $PhCH_2$, **18**; R = $SiMe_3$, **19**]. The three carbene complexes **17**−**19** display quite an unusual high-spin state, which is a consequence of the formation of a weak π interaction between the metal and the carbene carbon, as confirmed by the extended Hückel calculations. The carbene functionality has been removed from the iron center in the reaction with O_2 and HCl. The proposed structures have been supported by X-ray analyses of complexes **8**, **9**, **12**, **14**, **16**, **17**, and **19**.

Introduction

Although a variety of chemical transformations are assisted or catalyzed by iron−oxo surfaces,[1] their simulation by iron compounds is almost nonexistent. One preliminary attempt would be to disclose how much an oxygen donor atom environment can affect the redox properties of the iron center and its tendency to form iron−carbon bonds.[2,3] To this purpose, we have considered as ligand the bisalkylated calix[4]arene dianion (Chart 1). This ligand has a number of characteristics making the simulation of an oxo surface very likely:[4−6] (i) the preorganized quasi-planar arrangement of four oxygen donor atoms; (ii) the cavity and the substituents at the two oxygen atoms can be used for protecting the accessibility to the axial positions of square planar iron; (iii) the presence of two weakly binding ether groups can mimic variation in the coordination

* To whom correspondence should be addressed.

(1) (a) Thomas, J. M.; Thomas, W. J. *Principles and Practice of Heterogeneous Catalysis*; VCH: Weinheim, Germany, 1997. (b) *Mechanisms of Reactions of Organometallic Compounds with Surfaces*; Cole-Hamilton, D. J., Williams, J. O., Eds.; Plenum: New York, 1989. (c) Kung, H. H. *Transition Metal Oxides: Surface Chemistry and Catalysis*; Elsevier: Amsterdam, The Netherlands, 1989. (d) Hoffmann, R. *Solid and Surfaces, A Chemist's View of Bonding in Extended Strucures*; VCH: Weinheim, Germany, 1988. (e) *Catalyst Design, Progress and Perspectives*; Hegedus, L., Ed.; Wiley: New York, 1987. (f) Bond, G. C. *Heterogeneous Catalysis, Principles and Applications*, 2nd ed.; Oxford University Press: New York, 1987.

(2) For related molecular approaches to oxo surfaces binding organometallic functionalities see the following. (a) Chisholm, M. H. *Chemtracts: Inorg. Chem.* **1992**, *4*, 273. (b) Kläui, W. *Angew. Chem., Int. Ed. Engl.* **1990**, *29*, 627. (c) Nagata, T.; Pohl, M.; Weiner, H.; Finke, R. G. *Inorg. Chem.* **1997**, *36*, 1366. (d) Pohl, M.; Lyon, D. K.; Mizuno, N.; Nomiya, K.; Finke, R. G. *Inorg. Chem.* **1995**, *34*, 1413.

(3) Silver, J. *Chemistry of Iron*; Blackie: Glasgow, U.K., 1993. Pearson, A. J. *Iron Compounds in Organic Synthesis*; Academic: New York, 1994. Whitmire, K. H.; Kerber, R. C.; Fagan, P. J.; Akita, M. In *Comprehensive Organometallic Chemistry II*; Abel, E. W., Stone, F. G. A., Wilkinson, G., Eds.; Pergamon: Oxford, 1995; Vol. 7, Chapters 1−4.

(4) Floriani, C. *Chem.—Eur. J.* **1999**, *5*, 19.

(5) (a) Giannini, L.; Caselli, A.; Solari, E.; Floriani, C.; Chiesi-Villa, A.; Rizzoli, C.; Re, N.; Sgamellotti, A. *J. Am. Chem. Soc.* **1997**, *119*, 9198. (b) Giannini, L.; Caselli, A.; Solari, E.; Floriani, C.; Chiesi-Villa, A.; Rizzoli, C.; Re, N.; Sgamellotti, A. *J. Am. Chem. Soc.* **1997**, *119*, 9709. (c) Caselli, A.; Giannini, L.; Solari, E.; Floriani, C.; Re, N.; Chiesi-Villa, A.; Rizzoli, C. *Organometallics* **1997**, *16*, 5457. (d) Zanotti-Gerosa, A.; Solari, E.; Giannini, L.; Floriani, C.; Re, N.; Chiesi-Villa, A.; Rizzoli, C. *Inorg. Chim. Acta* **1998**, *270*, 298. (e) Castellano, B.; Solari, E.; Floriani, C.; Re, N.; Chiesi-Villa, A.; Rizzoli, C. *Organometallics* **1998**, *17*, 2328. (f) Castellano, B.; Solari, E.; Floriani, C.; Re, N.; Chiesi-Villa, A.; Rizzoli, C. *Chem. Eur. J.* **1999**, *5*, 722. (g) Castellano, B.; Solari, E.; Floriani, C.; Scopelliti, R.; Re, N. *Inorg. Chem.* **1999**, *38*, 3406.

10.1021/ic991467h CCC: $19.00 © 2000 American Chemical Society
Published on Web 05/18/2000

Chart 1

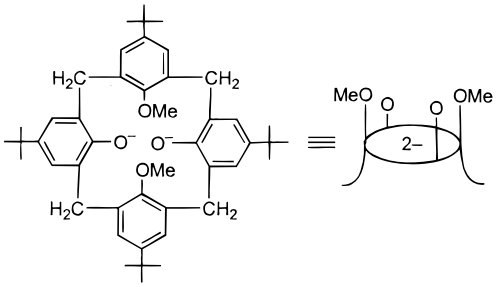

number of the metal according to the nature of the axial ligands. In this report we focus on the synthesis of the iron(II) dimethoxycalix[4]arene parent compound, its oxidation to iron(III) derivatives, and the formation of iron−carbon multiple bonds[7] in carbene and isocyanide derivatives.

Experimental Section

General Procedure. All reactions were carried out under an atmosphere of purified nitrogen. Solvents were dried and distilled before use by standard methods. Infrared spectra were recorded with a Perkin-Elmer FT 1600 spectrophotometer. NMR spectra were recorded on an AC-200 Bruker spectrometer. Elemental analyses were performed using an EA 1110 CHN elemental analyzer by CE Instruments. Unless otherwise indicated, all commercial reagents were used as received. Compounds **1**−**3**,[8] Ph_2CN_2,[9] and $[Fe_2Mes_4]$[10] were prepared according to published procedures. The solvent content of the solids has been confirmed, in many cases, by CG analysis of the products derived from their thermal decomposition.

Magnetic susceptibility measurements were made on a MPMS5 superconducting quantum interference device susceptometer (Quantum Design Inc.) operating at a magnetic field strength of 1 kOe. Corrections were applied for diamagnetism calculated from Pascal constants.[11] Effective magnetic moments were calculated as $\mu_{eff} = 2.828(\chi_V T)^{1/2}$, where χ_V is the magnetic susceptibility per vanadium. Fitting of the magnetic data to the theoretical expression was performed by minimizing the agreement factor, defined as $\sum[\chi_i^{obsd}T_i - \chi_i^{calcd}T_i]^2/(\chi_i^{obsd}T_i)^2$ through a Levenberg−Marquardt routine.

Extended Hückel Calculations. Extended Hückel calculations were performed with the CACAO molecular orbital program,[12] with parameters taken from ref 13.

Synthesis of 4. *N*,*O*-bis(trimethylsilyl)acetamide (BSA) (36.1 mL, 147.6 mmol) was rapidly added to a CH_3CN suspension (800 mL) of *p*-Bu^t−calix[4]arene•(CH_2Cl_2) (98.49 g, 134.2 mmol) under a stream of nitrogen while stirring. A white microcrystalline solid formed immediately, and the suspension was stirred a few minutes, by which time all starting material had been consumed. The solid was collected and dried (10^{-6} mbar, 85 °C, 48 h), yielding **4** as a white fluffy powder (103 g, 97%). Anal. Calcd for $C_{50}H_{72}O_4Si_2$: C, 75.70; H, 9.15. Found: C, 75.55; H, 9.12. ^{1}H NMR (C_6D_6, 200 MHz, 298 K, ppm): δ 8.12 (s, 2H, OH); 7.23 (s, 4H, ArH); 6.95 (s, 4H, ArH); 4.50 (d, 4H, J = 13 Hz $ArCH_2Ar$); 3.32 (d, 4H, J = 13 Hz $ArCH_2Ar$); 1.46 (s, 18H, $C(CH_3)$; 0.87 (s, 18H, $C(CH_3)$ 0.36 (s, 18H, $Si(CH_3)$. ^{1}H NMR ($CDCl_3$, 200 MHz, 298 K, ppm): δ 7.17 (s, 2H, OH); 7.02 (s, 4H, ArH); 6.75 (s, 4H, ArH); 4.22 (d, 4H, J = 13 Hz, $ArCH_2Ar$); 3.19 (d, 4H, J = 13 Hz $ArCH_2Ar$); 1.51 (s, 18H, $C(CH_3)$; 1.20 (s, 18H, $C(CH_3)$; 0.37 (s, 18H, $Si(CH_3)$. X-ray quality crystals were grown in $CHCl_3$/MeOH solutions.

Synthesis of 5. $[Fe_2Mes_4]$ (9.19 g, 15.65 mmol) was added to a pale-yellow solution of **1** (21.20 g, 31.3 mmol) in THF (230 mL). The resulting red suspension was stirred for 12 h during which time it gradually become a brown suspension with a microcrystalline precipitate in a slightly exothermic process. Volatiles were distilled off, and *n*-pentane (110 mL) was added to the solid residue. **5** was collected as a white powder (22.24 g, 89%). Anal. Calcd for $C_{50}H_{66}FeO_5$: C, 74.80; H, 8.28. Found: C, 74.99; H, 8.27.

Synthesis of 6. $[Fe_2Mes_4]$ (2.50 g, 4.25 mmol) was added to a pale-yellow solution of **2** (6.48 g, 8.51 mmol) in THF (120 mL), and the resulting red solution was stirred for 18 h. A brown solution was obtained. Volatiles were distilled off, and *n*-pentane (40 mL) was added to the solid residue. **6** was collected as a white powder (6.05 g, 80%). Anal. Calcd for $C_{56}H_{78}FeO_5$: C, 75.82; H, 8.86. Found: C, 75.71; H, 8.92.

Synthesis of 7. $[Fe_2Mes_4]$ (5.46 g, 9.27 mmol) was added to a solution of **3** (15.38 g, 18.55 mmol) in THF (200 mL), and the resulting red suspension was stirred overnight. A brown solution was obtained. Volatiles were distilled off, and *n*-pentane (110 mL) was added to the solid residue. **7** was collected as a white powder (14.43 g, 81%). Anal. Calcd for $C_{62}H_{74}FeO_5$: C, 77.97; H, 7.81. Found: C, 77.87; H, 7.95.

Synthesis of 8. $[Fe_2Mes_4]$ (6.43 g, 10.91 mmol) was added to a solution of **4** (17.32 g, 21.83 mmol) in THF (230 mL), and the resulting red suspension was stirred for 4 h during which time it gradually become a brown solution. Volatiles were distilled off, and *n*-pentane (90 mL) was added to the solid residue. **8** was collected as a white powder (15.77 g, 85%). Anal. Calcd for $C_{50}H_{70}FeO_4Si_2$: C, 70.89; H, 8.33. Found: C, 70.80; H, 8.51. X-ray quality crystals were grown in toluene solutions.

Synthesis of 9 (Method A). $HgCl_2$ (905 mg, 3.33 mmol) was added to a clear-green solution of **5** (2.68 g, 3.33 mmol) in toluene (100 mL), resulting immediately in a deep-purple suspension. A portion of insoluble material was filtered off (HgCl), while the filtrate was concentrated to dryness, leaving a deep-purple solid residue to which *n*-pentane (40 mL) was added. Complex **9**•$(thf)_2$ was collected as a deep-purple powder (1.84 g, 61%). Anal. Calcd for $C_{54}H_{74}ClFeO_6$: C, 71.24, H, 8.19. Found: C, 70.86, H, 7.87. X-ray quality crystals were grown in Et_2O/toluene solution. The crystals contain Et_2O and toluene of crystallization.

Synthesis of 9 (Method B). $PhCH_2Cl$ (248 mg, 1.96 mmol) was rapidly added to a stirred clear-green solution of **5** (1.57 g, 1.96 mmol) in toluene (100 mL), resulting immediately in a deep-purple solution. Volatiles were distilled off, leaving a deep-purple solid residue to which *n*-pentane (40 mL) was added. Complex **9**•$(toluene)_{0.5}$ was collected as a deep-purple powder (1.05 g,65%). Anal. Calcd for $C_{49.5}H_{62}ClFeO_4$: C, 73.19, H, 7.69. Found: C, 73.18, H, 7.96.

Synthesis of 10. Iodine (370 mg, 1.46 mmol) was added to a clear-green solution of **5** (2.34 g, 2.91 mmol) in toluene (100 mL). The resulting deep-violet solution was stirred overnight. Volatiles were distilled off, and *n*-pentane (40 mL) was added to the solid residue. Complex **10** was collected as a deep-violet powder (1.55 g, 62%). Anal. Calcd for $C_{46}H_{58}FeIO_4$: C, 64.42, H; 6.82. Found: C, 64.58; H, 6.90.

Synthesis of 11. A clear-green solution of **5** (4.816 g, 6.00 mmol) in toluene (100 mL) was cooled to −30 °C and exposed to purified O_2 while being stirred. The color gradually turned deep-red, and in few minutes a red precipitate appeared. After 12 h O_2 was replaced with N_2 and the suspension was allowed to warm to room temperature. Volatiles were distilled off, and *n*-pentane (80 mL) was added to the red residue. Complex **11**•(C_5H_{12}) was collected as a red powder (2.88

(6) (a) Giannini, L.; Solari, E.; Dovesi, S.; Floriani, C.; Re, N.; Chiesi-Villa, A.; Rizzoli, C. *J. Am. Chem. Soc.* **1999**, *121*, 2784. (b) Giannini, L.; Guillemot, G.; Solari, E.; Floriani, C.; Re, N.; Chiesi-Villa, A.; Rizzoli, C. *J. Am. Chem. Soc.* **1999**, *121*, 2797. (c) Giannini, L.; Dovesi, S.; Solari, E.; Floriani, C.; Chiesi-Villa, A.; Rizzoli, C. *Angew. Chem., Int. Ed.* **1999**, *38*, 807. (d) Giannini, L.; Solari, E.; Floriani, C.; Re, N.; Chiesi-Villa, A.; Rizzoli, C. *Inorg. Chem.* **1999**, *38*, 1438. (e) Dovesi, S.; Solari, E.; Scopelliti, R.; Floriani, C. *Angew. Chem., Int. Ed. Engl.* **1999**, *38*, 2388. (f) Caselli, A.; Solari, E.; Scopelliti, R.; Floriani, C. *J. Am. Chem. Soc.* **1999**, *121*, 8296.

(7) A preliminary communication on the Fe−calixarene carbene functionality has been published. Giusti, M.; Solari, E.; Giannini, L.; Floriani, C.; Chiesi-Villa, A.; Rizzoli, C. *Organometallics* **1997**, *16*, 5610.

(8) Arduini, A. Casnati, A. In *Macrocycle Synthesis*; Parker, P., Ed.; Oxford University Press: New York, 1996; Chapter 7.

(9) Smith, L. I.; Howard, K. L. *Organic Syntheses*; Wiley: New York, 1955; Vol. 3, p 351.

(10) Klose, A.; Solari, E.; Floriani, C.; Chiesi-Villa, A.; Rizzoli, C.; Re, N. *J. Am. Chem. Soc.* **1994**, *116*, 9123.

(11) Boudreaux, E. A.; Mulay, L. N. *Theory and Applications of Molecular Paramagnetism*; Wiley: New York, 1976; pp 491−495.

(12) Mealli, C.; Proserpio, D. M. *J. Chem. Educ.* **1990**, *67*, 3399.

(13) Alvarez, S. *Tables of Prameters for Extended Hückel Calculations*; Universitat de Barcelona: Barcelona, Spain, 1993.

g, 67%). Anal. Calcd for $C_{97}H_{128}Fe_2O_9$: C, 75.18; H, 8.32. Found: C, 75.11; H, 8.32. X-ray quality crystals were grown in toluene solutions.

Synthesis of 12. A clear, green-brown solution of **6** (5.694 g, 6.99 mmol) in toluene (100 mL) was cooled to −30 °C and exposed to purified O_2 while being stirred. The color gradually turned deep-red. After 6 h O_2 was replaced with N_2 and the suspension was allowed to warm to lab temperature. Volatiles were distilled off, and *n*-pentane (100 mL) was added to the red residue. Complex **12** was collected as a red powder (4.29 g, 75%). Anal. Calcd for $C_{104}H_{140}Fe_2O_9$: C, 75.88; H, 8.57. Found: C, 75.77; H, 8.74. X-ray quality crystals were grown in toluene solutions.

Synthesis of 13. Sulfur (109 mg, 0.43 mmol) was added to a clear-green solution of **5** (2.34 g, 2.91 mmol) in toluene (100 mL), and the resulting deep-violet solution was stirred overnight. Volatiles were distilled off, and *n*-pentane (40 mL) was added to the solid residue. Complex **13** was collected as a deep-violet powder (1.92 g, 76%). Anal. Calcd for $C_{92}H_{116}Fe_2O_8S$: C, 73.98, H, 7.83. Found: C, 73.90; H, 7.81.

Synthesis of 14. A brown solution of **7** (2.34 g, 2.44 mmol) in Et_2O (100 mL) was cooled to −30 °C and exposed to purified O_2 while being stirred. The color gradually turned deep-red. After 8 h O_2 was replaced with N_2 and the suspension was allowed to warm to room temperature. Volatiles were distilled off, and *n*-pentane (30 mL) was added to the orange residue. Complex **14** was collected as an orange powder (1.30 g, 67%). Anal. Calcd for $C_{51}H_{59}FeO_4$: C, 77.36; H, 7.51. Found: C, 77.49; H, 7.92. X-ray quality crystals were grown in toluene solutions.

Synthesis of 15. A brown solution of **8** (4.14 g, 4.89 mmol) in Et_2O (120 mL) was cooled to −30 °C and exposed to purified O_2 while stirring. The color gradually turned deep-purple, and a crystalline precipitate formed. After 12 h O_2 was replaced with N_2 and the suspension was allowed to warm to lab temperature. Volatiles were distilled off, and *n*-pentane (30 mL) was added to the solid residue. Complex **15**·$(Et_2O)_{1.5}$ was collected as a deep-purple powder (2.06 g, 47.6%). Anal. Calcd for $C_{53}H_{76}FeO_{5.5}Si$: C, 71.92; H, 8.65. Found: C, 71.97; H, 8.32. X-ray quality crystals were grown in toluene solutions.

Synthesis of 16. Complex **8** (3.25 g, 3.84 mmol) was added to a toluene solution (100 mL) of Bu^tNC (638 mg, 7.67 mmol), and the resulting deep-yellow solution was stirred overnight. Volatiles were distilled off, and *n*-pentane (110 mL) was added to the solid residue. Complex **17** was collected as a yellow powder (2.50 g, 64%). Anal. Calcd for $C_{55}H_{79}FeNO_4Si_2$: C, 71.09, H, 9.05; N, 1.51. Found: C, 71.01, H, 8.57; N, 1.53. IR (Nujol, ν_{max}/cm^{-1}): 2175 (m). X-ray quality crystals were grown in THF/toluene solutions.

Synthesis of 17. Solid Ph_2CN_2 (0 °C, 691 mg, 3.56 mmol) was added in one portion to a cold (−30 °C), clear-green solution of **5** (2.86 g, 3.56 mmol) in toluene (100 mL). The color turned quite soon to deep-green. It was allowed to warm to lab temperature over 5 h. Volatiles were distilled off, and *n*-pentane (40 mL) was added to the green residue. Complex **17** was collected as a green powder (2.59 g, 81%). Anal. Calcd for $C_{59}H_{68}FeO_4$: C, 79.00; H, 7.64. Found: C, 78.98; H, 7.51. Crystals suitable for X-ray analysis were obtained from CH_2Cl_2.

Synthesis of 18. Complex **7** (2.98 g, 3.11 mmol) was added in one portion to a cold (−30 °C) solution of Ph_2CN_2 (654 mg, 3.37 mmol) in *n*-hexane (80 mL). The resulting deep-red suspension was stirred for 2 h, then allowed to come to room temperature over 5 h, during which time it gradually turned deep-green. The precipitate was collected and dried, yielding **18** as a green powder (2.46 g, 75%). Anal. Calcd for $C_{71}H_{76}FeO_4$: C, 81.28; H, 7.30. Found: C, 80.99; H, 7.02. Sometimes the solid contains hydrocarbons of crystallization, i.e., C_6H_{14} or C_5H_{12}.

Synthesis of 19. Complex **8** (3.14 g, 3.71 mmol) was added in one portion to a cold (−30 °C) solution of Ph_2CN_2 (719 mg, 3.71 mmol) in *n*-pentane (80 mL). The resulting deep-red suspension was allowed to come to lab temperature over 5 h, during which time it gradually turned deep-green. The precipitate was collected and dried, yielding **19** as a green powder (1.61 g, 43%). Anal. Calcd for $C_{63}H_{80}FeO_4Si_2$: C, 74.67; H, 7.98. Found: C, 74.24; H, 7.77. Crystals suitable for X-ray analysis were obtained from a pentane solution.

Synthesis of 20. Pyridinium chloride (0.38 g, 3.31 mmol) was added in one portion to a solution of **18** (C_5H_{12}) (3.51 g, 3.63 mmol) in Et_2O (150 mL), and the resulting deep-green solution was stirred for 36 h at which time a pale-green precipitate was obtained. It was collected and dried as a pale green powder, **20** (2.29 g, 68%). Anal. Calcd for $C_{64}H_{74}ClFeNO_4$: C, 75.91; H, 7.37; N, 1.38. Found: C, 76.01; H, 7.26; N, 1.12.

Scheme 1

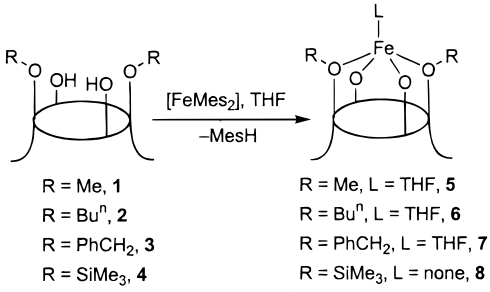

Reaction of 17 with O_2. A solution of **17**·(C_5H_{12}) (3.17 g, 3.28 mmol) in toluene (100 mL) was exposed to purified O_2 while being stirred. The starting green solution gradually turned deep-amber. Volatiles were distilled off, and *n*-pentane (40 mL) was added to the red residue. Complex **11**·$(C_5H_{12})_2$ was collected as a red powder (2.14 g, 80%). Anal. Calcd for $C_{102}H_{140}Fe_2O_9$: C, 75.54; H, 8.70. Found: C, 75.76; H, 8.35. Benzophenone was obtained as a byproduct in a stoichiometric amount. A gas absorption measurement gave a molar ratio Fe/O_2 of $^2/_3$.

X-ray Crystallography for Complexes 8, **9, 12, 14, 16, 17, and 19**. Single crystals suitable for X-ray diffraction were grown from common organic solvents (Table 1). Data for **8** and **16** were collected on a Kuma KM4CCD, data for **17** were collected on a Rigaku AFC6S diffractometer, and those for **9**, **12**, **14**, and **19** were collected on a MAR345 image plate using Mo Kα radiation. The solutions and refinements were carried out using the programs SHELX76[14] and SHELX93.[15] The details of the X-ray data collection, structure solution, and refinement are given in the Supporting Information.[16]

Results and Discussion

(A) Starting Compounds: [Fe{*p*-Bu^t−calix[4]−$(O)_2(OR)_2$]. The Experimental Section details the large-scale synthesis of the bisalkylated derivatives of *p*-Bu^t−calix[4]arene, namely, *p*-Bu^t−calix[4]−$(O)_2(OR)_2$ (**1**−**4**), which are not available from the literature.[8] The use of the bisalkylated form is compulsory for three major reasons: (i) for binding iron in its +2 oxidation state, (ii) for keeping a coordination site or a metal functionality available for reactivity studies, and (iii) for protecting the [FeO_4] moiety from dimerization, which prevents reactivity at the metal center.[17]

The parent complexes **5**−**8** are easily accessible from the reaction of the free ligands **1**−**4** and [Fe_2Mes_4][10] (Scheme 1). The alternative synthesis from $FeCl_2$ and the alkali salts of **1**−**4** should not be pursued because of the difficulty in freeing the final complex from [MCl], particularly when [Cl^-] remains bonded to iron(II) (see below, complex **20**). Depending on the nature of R, the iron(II)−calix[4]arene complexes can be obtained in the unsolvated (complex **8**) or solvated (**5**−**7**) form, though in the latter case the solvent molecule is only weakly bonded. All monomeric complexes **5**−**8** display a magnetic behavior according to a d^6 high-spin state (see below). The structures of **5**−**8** are exemplified by a report on the X-ray

(14) Sheldrick, G. M. *SHELX76, program for crystal structure determination*; University of Cambridge: Cambridge, England, 1976.
(15) Sheldrick, G. M. *SHELXL*93, *program for crystal structure refinement*; University of Göttingen: Göttingen, Germany, 1993.
(16) See paragraph at the end of paper regarding Supporting Information.
(17) Olmstead, M. M.; Sigel, G.; Hope, H.; Xu, X.; Power, P. P. *J. Am. Chem. Soc.* **1985**, *107*, 8087.

Table 1. Experimental Data for the X-ray Diffraction Studies of Crystalline Complexes **8**, **9**, **12**, **14**, **16**, **17**, and **19**

complex	**8**	**9**	**12**	**14**	**16**	**17**	**19**
formula	$C_{50}H_{70}FeO_4Si_2\cdot C_7H_8$	$C_{46}H_{58}ClFeO_4\cdot 0.5C_7H_8\cdot 0.5C_4H_{10}O$	$C_{104}H_{140}Fe_2O_9$	$C_{102}H_{118}Fe_2O_8\cdot 4C_7H_8$	$C_{55}H_{79}FeNO_4Si_2\cdot C_4H_8O$	$C_{59}H_{68}FeO_4\cdot 3CH_2Cl_2$	$C_{63}H_{80}FeO_4Si_2$
a, Å	21.759(3)	16.969(3)	19.295(4)	12.648(3)	12.283(2)	13.115(2)	11.195(2)
b, Å	19.105(3)	13.510(3)	20.942(4)	13.492(3)	14.951(2)	21.265(3)	21.762(4)
c, Å	12.776(2)	21.526(4)	24.841(5)	18.286(4)	18.122(2)	12.573(2)	25.408(4)
α, (deg)	90	90	90	83.68(3)	84.66(2)	100.57(2)	100.53(3)
β, (deg)	92.30(2)	107.61(3)	90	72.04(3)	80.03(2)	117.53(2)	97.59(1)
γ, (deg)	90	90	90	66.63(3)	66.54(2)	76.64(2)	89.68(3)
V, Å^3	5306.8(14)	4703.6(18)	10038(3)	2724.6(13)	3005.7(9)	3013.3(10)	6031.4(19)
Z	4	4	4	1	2	2	4
fw	939.3	849.4	1645.9	1952.3	1002.4	1151.8	1013.3
space group	C2/*c* (No. 15)	$P2_1/c$ (No. 14)	*Pbcn* (No. 60)	*P*1 (No. 2)	*P*1 (No. 2)	*P*1 (No. 2)	*P*1 (No. 2)
temp, °C	−130	−130	−130	−130	−130	−135	−130
λ, Å	0.710 69	0.710 69	0.710 69	0.710 69	0.710 69	0.710 69	0.710 69
ρ_{calc}, g cm^{-3}	1.176	1.200	1.089	1.190	1.108	1.270	1.116
μ, cm^{-1}	3.68	4.18	3.38	3.20	3.30	5.6	3.29
transm coeff	3.68	4.18	3.38	3.20	3.30	5.6	3.29
R^a	0.056	0.086	0.063	0.064	0.108	0.073	0.067
wR2	0.136	0.218	0.166	0.168	0.279	0.225	0.165
GOF	1.059	1.090	0.918	1.059	1.072	1.016	1.092
N obsd[c]	5069	5226	3532	7566	7758	3599	14 202
N-independent[d]	6211	9401	7483	10 888	10 248	8718	24 241
N-refinement [e]	5069	5226	6475	7566	7758	6941	14 202
variables	290	505	514	618	613	652	1258

[a] Calculated on the observed reflections. [b] Values in square brackets refer to the "inverted" structure. [c] *N*-obsd is the total number of independent reflections having $I > 2\sigma(I)$. [d] *N*-independent is the number of independent reflections. [e] *N*-refinement is the number of reflection used in the refinement having $I > 0$ for **12** and **17** and $I > 2\sigma(I)$ for **8**, **9**, **14**, **16**, **19**.

Scheme 2

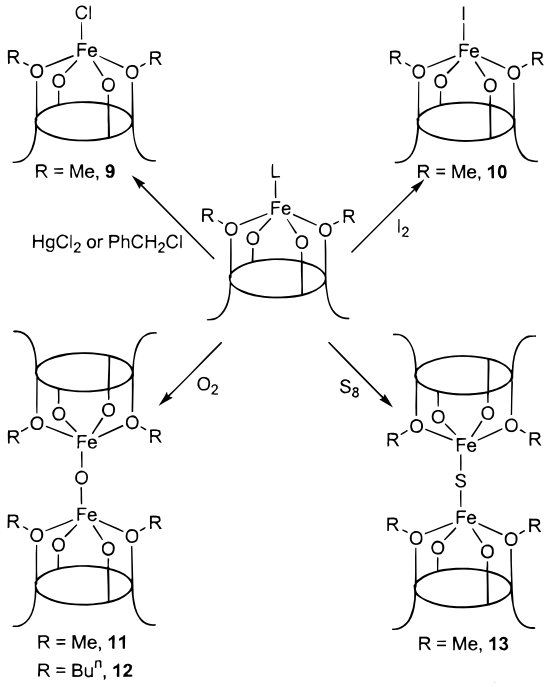

analysis of **8** (see below), while the structure of **5** is given in the Supporting Information.

(B) One-Electron Oxidation of [Fe{*p*-Bu^t−calix[4]−(O)$_2$-(OR)$_2$]. The parent compounds **5**−**8**, regardless of the coordination number of the metal, i.e., 4 or 5, are prone to be oxidized to iron(III) derivatives. Scheme 2 displays a number of these reactions, specifically the transformations to iron(III) halides and iron(III) oxo functionalities. The former reactions leading to **9** and **10** follow the usual free radical type pathway and give rise to five-coordinate iron(III) derivatives, displaying the typical high-spin state of a d^5. Complexes **9** and **10** are particularly appropriate for pursuing further functionalization of the iron center.

Chart 2

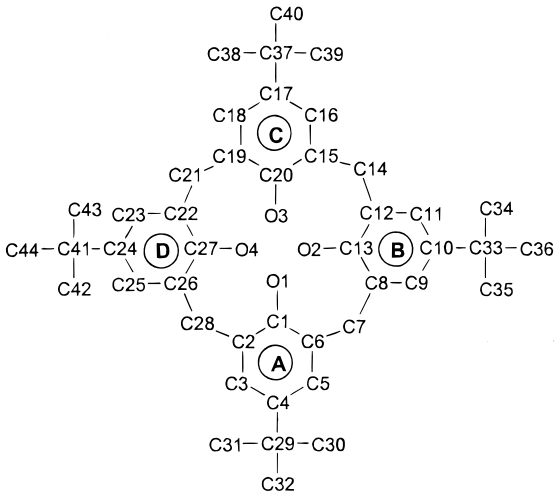

For discussing the X-ray structural analysis of the prototypes of each class of compounds reported in this paper, we refer to the numbering scheme in Chart 2 while a selection of the structural parameters of complexes **8**, **9**, **12**, **14**, **16**, **17**, and **19** is reported in Table 2 and the conformational parameters are listed in Table 3.

The structures of complexes **8** and **9** are displayed in Figures 1 and 2, respectively.[18] In complex **8** the O_4 core shows little, yet significant, tetrahedral distortions (Table 3). The macrocyclic ligand is square-planarly coordinated to iron, the metal out-of-plane distance being 0.010(1) Å. Complex **9** possesses a crystallographically imposed C_2 symmetry, the 2-fold axis running along the Fe−Cl(1) direction. The coordination polyhedron around the metal is nearly a trigonal bipyramid, with the O(1), O(3), Cl(1) atoms defining the equatorial plane and

(18) Complex **8** crystallizes with one toluene solvent molecule that is hosted in the calixarene cavity. The calixarene cavity of complex **9** is statistically occupied by toluene and Et_2O molecules in a complex/toluene/Et_2O molar ratio of 1/0.5/0.5.

Table 2. Selected Bond Distances (Å) and Angles (deg) for **8**, **9**, **12**, **14**, **16**, **17**, and **19**

8

Fe(1)−O(1)	1.825(2)	Fe(1)−O(2)	2.205(2)	Si(1)−O(2)	1.684(2)

9

Fe(1)−Cl(1)	2.235(1)	Fe(1)−O(1)	1.787(4)	Fe(1)−O(2)	2.208(4)
Fe(1)−O(3)	1.806(4)	Fe(1)−O(4)	2.168(3)		

12[a]

Fe(1)−O(1)	1.808(4)	Fe(1)−O(2)	2.214(4)	Fe(1)−O(3)	1.825(4)
Fe(1)−O(4)	2.207(4)	Fe(1)−O(5)	1.765(1)	Fe(1)−O(5)−Fe(1)′	177.3(1)

14[b]

Fe(1)−O(1)	1.782(3)	Fe(1)−O(2)	2.225(2)	Fe(1)−O(3)	1.831(3)
Fe(1)−O(4)	2.092(3)	Fe(1)−O(4)′	1.914(2)		

16

Fe(1)−O(1)	1.875(4)	Fe(1)−O(2)	2.396(4)	Fe(1)−O(3)	1.874(5)	Fe(1)−O(4)	2.381(5)
Fe(1)−C(51)	2.093(6)	Si(1)−O(2)	1.674(5)	Si(2)−O(4)	1.678(4)	N(1)−C(51)	1.152(8)
Fe(1)−C(51)−N(1)	179.2(5)						

17

Fe(1)−O(1)	1.852(5)	Fe(1)−O(2)	2.228(6)	Fe(1)−O(3)	1.831(4)	Fe(1)−O(4)	2.258(6)
Fe(1)−C(47)	1.943(8)	C(48)−C(47)	1.449(10)	C(54)−C(47)	1.485(10)		
Fe(1)−C(47)−C(54)	119.2(6)	Fe(1)−C(47)−C(48)	125.1(6)	C(48)−C(47)−C(54)	115.8(7)		

19

	molecule A	molecule B		molecule A	molecule B
Fe(1)−O(1)	1.818(2)	1.826(2)	Fe(1)−O(2)	2.203(2)	2.457(2)
Fe(1)−O(3)	1.807(3)	1.826(2)	Fe(1)−O(4)	2.915(2)	2.434(2)
Fe(1)−C(45)	1.958(5)	1.973(5)	Si(1)−O(2)	1.709(3)	1.689(2)
Si(2)−O(4)	1.667(3)	1.689(3)	C(46)−C(45)	1.464(6)	1.459(7)
C(52)−C(45)	1.469(7)	1.476(6)	Fe(1)−C(45)−C(52)	123.6(4)	121.3(4)
Fe(1)−C(45)−C(46)	118.2(4)	122.1(4)	C(46)−C(45)−C(52)	118.3(4)	116.6(4)

[a] ′ = $-x$, y, 1.5 − z. [b] ′ = $-x$, 1 − y, 1 − z.

Table 3. Comparison of Relevant Conformational Parameters within Calixarene for Complexes **8**, **9**, **12**, **14**, **16**, **17**, and **19**

							19	
	8	**9**	**12**	**14**	**16**	**17**	molecule A	molecule B
(a) Distances (Å) of Atoms from the O_4 Mean Plane[a]								
O(1)	0.185(2)	−0.232(3)	−0.252(4)	−0.361(2)	−0.169(4)	−0.209(4)	−0.274(3)	−0.229(3)
O(2)	−0.185(2)	0.229(3)	0.250(4)	0.339(2)	0.171(4)	0.212(4)	0.295(3)	0.229(3)
O(3)	0.185(2)	−0.230(3)	−0.249(4)	−0.310(2)	−0.173(4)	−0.218(4)	−0.296(3)	−0.232(3)
O(4)	−0.185(2)	0.233(3)	0.251(4)	0.332(2)	0.172(4)	0.215(4)	0.271(3)	0.232(3)
Fe	0.010(1)	0.478(1)	0.442(1)	0.407(1)	0.382(1)	0.553(2)	0.583(1)	0.552(1)
(b) Dihedral Angles (deg) between Planar Moieties[b]								
E−A	134.4(1)	133.8(1)	139.9(1)	152.5(1)	135.7(1)	131.9(2)	140.6(1)	137.0(1)
E−B	110.4(1)	109.1(1)	103.3(1)	114.1(1)	96.5(1)	111.6(3)	98.7(1)	97.8(1)
E−C	134.4(1)	134.6(1)	138.4(1)	125.4(1)	140.2(2)	133.4(1)	151.0(1)	139.7(1)
E−D	110.4(1)	118.1(1)	105.0(1)	112.8(1)	94.9(1)	110.2(2)	91.3(1)	98.8(1)
A−C	91.3(1)	91.5(1)	98.2(1)	97.9(1)	95.9(2)	94.7(2)	111.6(1)	96.7(1)
B−D	139.1(1)	132.8(2)	151.7(2)	133.0(1)	168.6(2)	137.6(3)	170.0(2)	163.4(2)
(c) Contact Distances (Å) between Para Carbon Atoms of Opposite Aromatic Rings[c]								
C(4)···C(17)	9.246(4)	9.102(8)	9.555(7)	9.358(5)	9.659(9)	8.971(10)	9.934(7)	9.524(7)
C(10)···C(24)	7.218(3)	7.565(6)	6.614(8)	7.558(5)	5.714(10)	7.365(15)	5.572(6)	6.034(7)

[a] For complex **8** O(30 and O(4) should be read O(1)′ and O(2)′, respectively; prime denotes a transformation of $-x$, y, 0.5 − z. [b] E (reference plane) refers to the least-squares mean plane defined by the C(7), C(14), C(21), C(28) bridging methylenic carbons. [c] For complex **8** C(17) and C(24) should be read C(4)′ and C(10)′, respectively; prime denotes a transformation of $-x$, y, 0.5 − z.

the O(2) and O(4) atoms at the axial positions. The metal is displaced by 0.028(1) Å from the equatorial plane. The Fe−Cl(1) vector forms a dihedral angle of 3.1(1)° with the normal to the O_4 mean plane. The short Fe−O(1) and Fe−O(3) bond distances in both **8** and **9** support a significant metal−oxygen π bonding, which is absent in the cases of O(2) and O(4) (Table 2). The calixarene macrocycles assume the usual elliptical conformation, the A and C rings being slightly pushed outward and the B and D rings inward, relative to the cavity (Table 3). The asymmetry of the cavity is monitored by the separation between the opposite C(4), C(17), and C(10), C(24) para carbon atoms. In this conformation a toluene molecule is accommodated inside the cavity as a guest.

The oxidation of **5**−**8** with dioxygen is strongly dependent on the R substituent at the alkylated oxygen (Scheme 2). In the case of Me and Bu^n the reaction led, independent of the reaction conditions, to the corresponding μ-oxo derivatives **11** and **12**. The latter compounds are similar to the μ-oxo derivatives of iron(III) supported by polydentate or macrocyclic ligands,[19] including the magnetic and structural properties (see below and

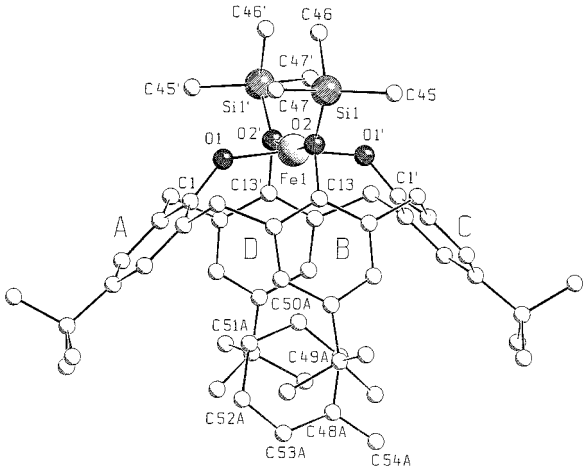

Figure 1. SCHAKAL view of complex **8**. Disorder affecting the toluene guest molecule has been omitted for clarity. A prime denotes a transformation of $-x, y, 0.5 - z$.

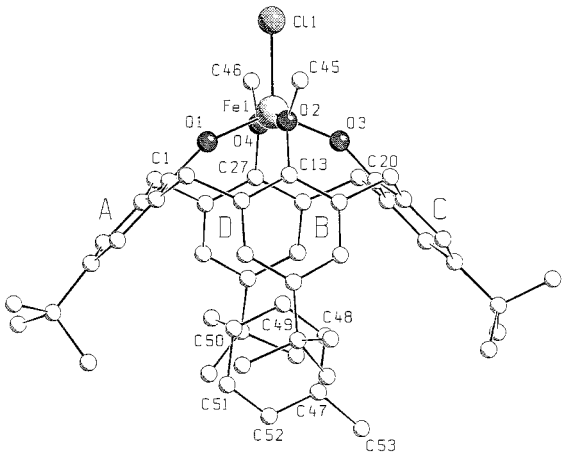

Figure 2. SCHAKAL view of complex **9**. Disorder involving the guest molecules has been omitted for clarity.

the Experimental Section). The reaction of **5** with elemental sulfur (Scheme 2) parallels the formation of the μ-oxo complex,[20,21] leading to **13**. An interesting comparison can be made between the magnetic properties of **11** and **13**. The reaction of **7** and **8** with dioxygen follows a completely different pathway, leading to the formation of the iron(III) dimers **14** and **15**. The reaction mechanism is rather difficult to determine, though a similar dealkylation has been observed whenever when we tried to increase the oxidation state or in general the specific charge of the metal (Scheme 3).[5] The antiferromagnetic properties of the iron(III) dimer have been analyzed and discussed in the following section. The structures of **12** and **14** are displayed in Figures 3 and 4.

Complex **12** (Figure 3) possesses a crystallographically imposed C_2 symmetry, the 2-fold axis running through the O(5) μ-oxo oxygen atom, perpendicular to the Fe−O(5)−Fe direction.

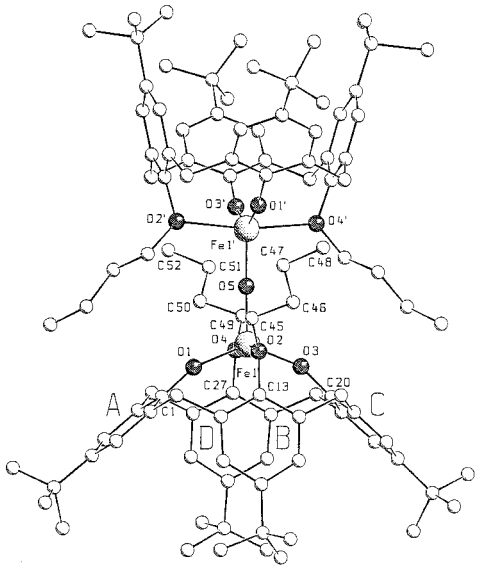

Figure 3. SCHAKAL view of complex **12**. Disorder affecting the B and D butyl groups has been omitted for clarity. A prime denotes a transformation of $-x, y, 1.5 - z$.

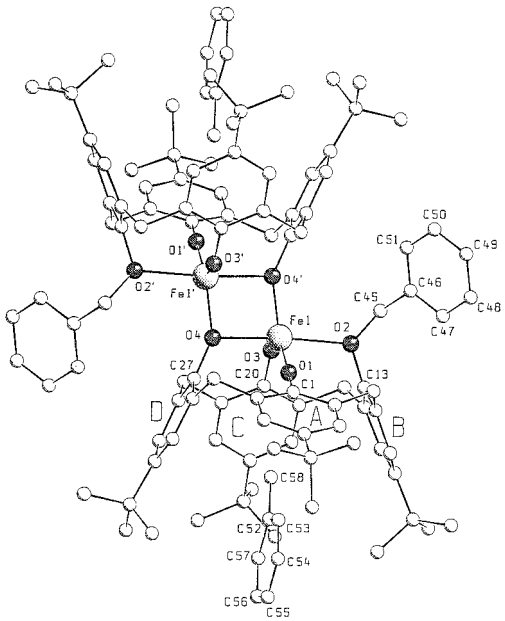

Figure 4. SCHAKAL view of complex **14**. A prime denotes a transformation of $-x, 1 - y, 1 - z$.

Scheme 3

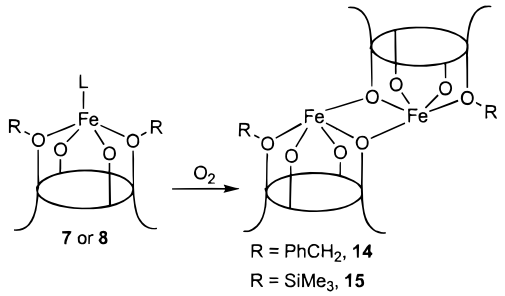

Complex **14** consists of centrosymmetric dimers (Figure 4). In both complexes iron exhibits five-coordination through the oxygen atoms of the tetrahedrally distorted O_4 core (Table 3) and the O(5) bridging oxo group in **12** or the O(4)′ oxygen atom from the symmetry-related calixarene in **14**. Both coordination

(19) (a) Kurtz, D. M., Jr. *Chem. Rev.* **1990**, *90*, 585 and references therein. (b) Haselhorst, G.; Wieghardt, K.; Keller, S.; Schrader, B. *Inorg. Chem.* **1993**, *32*, 520.

(20) Berno, P.; Floriani, C.; Chiesi-Villa, A.; Guastini, C. *J. Chem. Soc., Dalton Trans.* **1989**, 551.

(21) (a) Floriani, C.; Fachinetti, G. *Gazz. Chim. Ital.* **1973**, *103*, 1317. (b) Mitchell, P. C. H.; Parker, D. A. *J. Inorg. Nucl. Chem.* **1973**, *35*, 1385. Mitchell, P. C. H.; Parker, D. A. *J. Chem. Soc., Dalton Trans.* **1976**, 1821. (c) Dorfman, J. R.; Girerd, J. J.; Simhon, E. D.; Stack, T. D. P.; Holm, R. H. *Inorg. Chem.* **1984**, *23*, 4407 and references therein. (d) Corazza, F.; Floriani, C.; Zehnder, M. *J. Chem. Soc., Dalton Trans.* **1987**, 709.

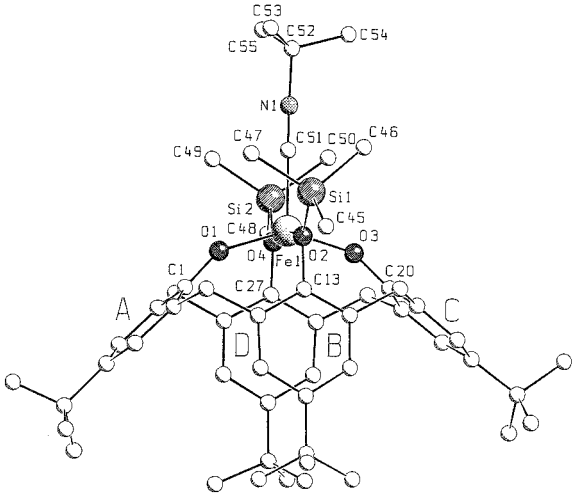

Figure 5. SCHAKAL view of complex **16**.

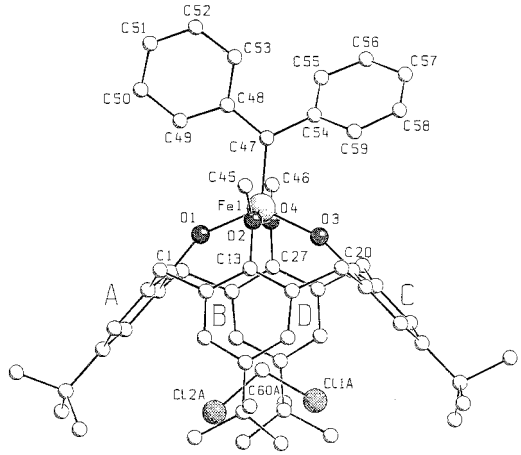

Figure 6. SCHAKAL view of complex **17**. Disorder affecting the C ring and the methylene chloride guest molecule has been omitted for clarity.

Scheme 4

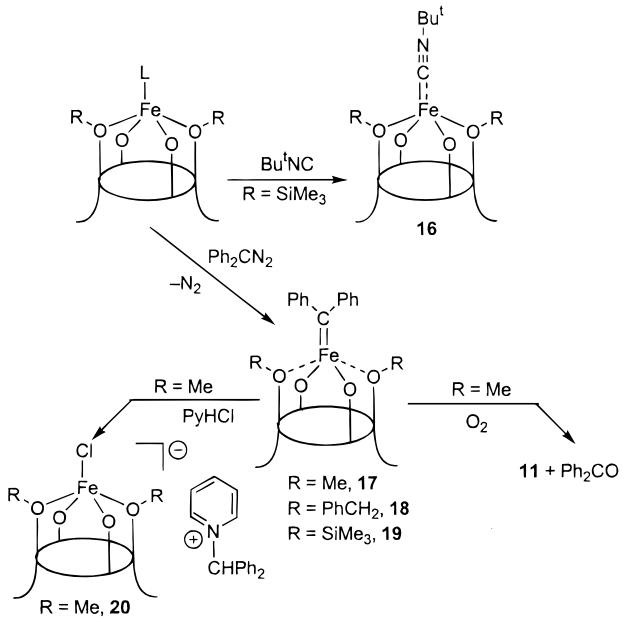

polyhedra resemble a trigonal bipyramid, with O(1), O(3), O(5) (in **12**) or O(1), O(3), O(4)′ (in **14**) defining the equatorial plane, while O(2) and O(4) are in the axial sites. The metal is displaced by 0.007(1) and 0.043(2) Å from the O_4 mean plane in **12** and **14**, respectively. The Fe−O(5) (**12**) and Fe−O(4)′ (**14**) vectors form dihedral angles of 11.3(1) and 1.3(1)°, respectively, with the normal to the corresponding O_4 mean planes. The Fe−O bond distances vary according to the degree of π-bonding formation between the metal and the different oxygen donor atoms. The elliptical conformation of the calixarene macrocycle is similar to those observed in the previous complexes,[5,6] the main difference consisting of the increase of the dihedral angle between the B and D rings in **12**.

(C) [Fe═C] Functionality. The synthetic approach to the Fe−C multiple bond functionalities has been devised by reacting **4**−**8** with Bu^{t}NC and diazoalkanes. The reaction of **8** with Bu^{t}NC led to the corresponding isocyanide derivative **16**, displaying a quite considerable increase in the C−N stretching vibration (2175 cm^{-1}), according to a highly electron-poor center. The structural parameters (Scheme 4) confirm a limited contribution by the iron ion to the formation of an Fe−C multiple bond. The reaction of the iron(II) complexes with diazoalkanes as the source of the corresponding carbenoids is quite appealing. The possibility of binding a carbene over a metal−oxo surface bears a particular significance because of the relationship with those surfaces active in the Fischer−Tropsch synthesis.[22] The reaction of **4**−**8**, regardless of the substituent at the oxygen atoms and the solvent bonded at the metal, led to the loss of N_2 from the diazoalkane. Only in the case, however, of diphenyldiazomethane was it possible to isolate quite stable carbene derivatives,[23] namely, **17**−**19**, which display an unusual thermal stability. Their reactivity is very limited toward conventional substrates like olefins and acetylenes. Although complexes **17**−**19** are quite stable, the synthesis of differently substituted carbenes, i.e., :CPhH, $(COOR)_2$C:, and (Ph)(COOR)C:, was unsuccessful.

The structures of **16**, **17**, and **19** are displayed in Figures 5, 6, and 7 and 8, respectively. In the crystals of **19** two crystallographically independent molecules showing a slightly different geometry are present. Hereafter, the two molecules will be referred as molecule **19A** (Figure 7) and **19B** (Figure 8). The five-coordination around iron is achieved through the four oxygen atoms from the calixarene and the C(51), C(47), and C(45) carbon atoms for **16**, **17**, and **19**, respectively. In all complexes the O_4 core shows remarkable tetrahedral distortions (Table 3), so the coordination polyhedron around the metals should be better described as a distorted trigonal bipyramid with the O(2), O(4), C(51); O(1), O(3), C(47); and O(1), O(3), C(45) atoms defining the equatorial plane for **16**, **17**, and **19**, respectively. The distortions from an ideal symmetry is mainly indicated by the value of the angles involving the apical oxygen

(22) Herrmann, W. A. In *Applied Homogeneous Catalysis with Organometallic Compounds*; Cornils, B., Herrmann, W. A., Eds.; VCH: Weinheim, Germany, 1996; Vol. II, Chapter 3, pp 747−762.

(23) For iron(II)−carbene functionality supported by a porphyrin ligand see the following. (a) Mansuy, D.; Lange, M.; Chottard, J. C.; Bartoli, J. F.; Chevrier, B.; Weiss, R. *Angew. Chem.* **1978**, *90*, 828. (b) Mansuy, D. *Pure Appl. Chem.* **1980**, *52*, 681. (c) Latos-Grazynski, L.; Cheng, R.-J.; La Mar, G. N.; Balch, A. L. *J. Am. Chem. Soc.* **1981**, *103*, 4270. (d) Balch, A. L.; Cheng, R.-J.; La Mar, G. N.; Latos-Grazynski, L. *Inorg. Chem.* **1985**, *24*, 2651. (e) Brothers, P. J.; Collman, J. P. *Acc. Chem. Res.* **1986**, *19*, 209. (f) Mansuy, D. *Pure Appl. Chem.* **1987**, *59*, 759. (g) Artaud, I.; Gregoire, N.; Battioni, J.-P.; Dupre, D.; Mansuy, D. *J. Am. Chem. Soc.* **1988**, *110*, 8714. (h) Artaud, I.; Gregoire, N.; Leduc, P.; Mansuy, D. *J. Am. Chem. Soc.* **1990**, *112*, 6899. (i) Wolf, J. R.; Hamaker, C. G.; Djukic, J.-P.; Kodadek, T.; Woo, L. K. *J. Am. Chem. Soc.* **1995**, *117*, 9194. (j) Ziegler, C. J.; Suslick, K. S. *J. Am. Chem. Soc.* **1996**, *118*, 5306. (k) Mansuy, D.; Mahy, J. P. In *Metalloporphyrins Catalyzed Oxidations*; Montanari, F., Casella, L., Eds.; Kluwer: Dordrecht, The Netherlands, 1994; p 175.

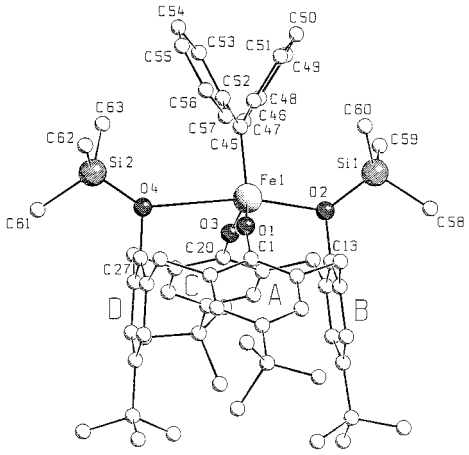

Figure 7. SCHAKAL view of molecule A in complex **19**.

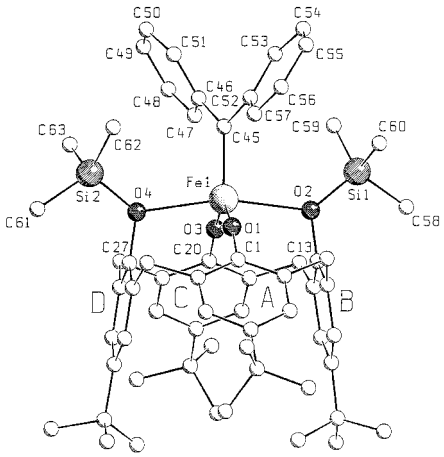

Figure 8. SCHAKAL view of molecule B in complex **19**. Disorder affecting the D ring has been omitted for clarity.

atoms [O(1)−Fe−O(3), 169.8(1)° in **16**; O(2)−Fe−O(4), 162.6(2) and 164.9(1)° in **17** and **19A**, respectively]. The metal is displaced by 0.017(2), 0.037(1), 0.251(2), and 0.004(2) Å from the O_4 cores of **16**, **17**, **19A**, and **19B**, respectively. The Fe−C(51), Fe−C(47), and Fe−C(45) vectors are nearly perpendicular to the O_4 core, and the dihedral angles are formed with the normal top, the O_4 mean planes being 1.1(2), 3.4(2), 7.4(2), and 0.60(2)° for **16**, **17**, **19A**, and **19B**, respectively. The shortest Fe−O bond distances (Table 2) correspond to the formation of significant π bonding, in agreement with the approximate linearity of the Fe−O−C bond angles [ranging from 150.1(4) to 172.1(3)° for Fe−O(1)−C(1) in **16** to Fe−O(3)−C(20) in **19A**, respectively]. A large difference has been observed in the Fe−O(2) distance between **19A** and **19B** [2.203(2) vs 2.457(2) Å]. The Fe−C bond distances involving both the isocyanide ligand (2.093(6) Å, complex **16**) and the carbene ligands (1.943(8), 1.958(5), 1.973(5) Å for complexes **17**, **19A**, and **19B**, respectively) are remarkably longer than the values usually observed.[23,24] In complexes **17** and **19** this lengthening could be ascribed to the intraligand steric hindrance involving α hydrogen atoms of the carbene phenyl rings and the O(1) and O(3) deprotonated oxygen atoms (complex **16**, O(1)···H(49), 2.39 Å; O(3)···H(59), 2.59 Å; complex **19A**, O(1)···H(47), 2.52 Å, O(3)···H(57), 2.38 Å; complex **19B**, O(1)···H(47), 2.49 Å, O(3)···H(57), 2.49 Å). As usually observed in disubstituted calixarene metal derivatives, the macrocycle assumes an elliptical cross section conformation,[5,6] as indicated by the dihedral angles the aromatic rings form with the "reference" plane and by the values of the distances between opposite para carbon atoms (Table 3).

The diphenylcarbene derivatives **17**−**19** are characterized by a very high thermal stability and kinetic inertness. They can be decomposed only by acids or oxygen. In the former case, the anionic iron(II) complex **20** has been obtained from the reaction of **17** with PyHCl. The protonation of the carbene carbon is followed by the homolytic cleavage of the Fe−C σ bond, thus forming the pyridinium cation $[PyCHPh_2]^+$, **20**. It should be mentioned at this stage that there was intrinsic instability of the Fe−C σ bond when we tried the alkylation of complexes **9** and **10**. The structure of **20** has been supported by X-ray analysis, which is not included in the present report because the structural parameters of the anion are quite similar to those of **9**. The reaction of **17** with O_2 produces benzophenone and the dianion μ-oxo complex **11**. The same reaction has been observed for other metal−carbene functionalities supported by macrocyclic ligands.[25]

(D) Magnetic Susceptibility Analysis. The magnetic susceptibilities of complexes **5**−**19** were measured in the temperature range 1.9−300 K, and those of **11**, **13**, and **14** are shown in Figure 9 as a function of temperature.

(D.1) Iron(II)−Iron(III) Complexes. The magnetic moments of **5**−**8** and **16**−**19** are essentially constant in the whole range of temperature, with room-temperature values of about 4.7−5.1 μ_B, and show only a small decrease below 20 K (due to zero-field splitting). This behavior is typical of high-spin, $S = 2$, Fe(II) monomeric species.[26]

The magnetic moments of **9** and **10** are constant in the whole range of temperature, with room-temperature values of ca. 5.9 μ_B, and are typical of high-spin, $S = {}^5/_2$, Fe(III) monomeric species.[26]

The temperature dependence of the magnetic moments of **11**−**15** shows a steady decrease from 300 to 1.9 K (Figure 9) and is typical of antiferromagnetic coupled Fe(III) dimers. The data for **11**, **13**, and **14** were fitted with a theoretical equation[26] based on the Heisenberg model $H = -2JS_1S_2$ ($S_1 = S_2 = {}^5/_2$):

$$\chi_{dim} = \frac{2Ng^2\mu_B{}^2}{kT}[\exp(x) + 5\exp(3x) + 14\exp(6x) + 30\exp(10x) + 55\exp(15x)]/[1 + 3\exp(x) + 5\exp(3x) + 7\exp(6x) + 9\exp(10x) + 11\exp(15x)]$$

where $\chi = J/(kT)$.

To obtain good fits, we included a correction for a small quantity of monomeric Fe(III) impurities that were assumed to obey Curie's law. The following equation is therefore used for the total susceptibility,

$$\chi = \frac{1}{2}(1-p)\chi_{dim} + p\frac{Ng'^2\mu_B{}^2S(S+1)}{3kT}$$

where $S = {}^5/_2$, g' is the g factor of the impurity (assumed to be 2.00), and p is the monomeric impurity fraction. The calculated best-fit parameters are $g = 1.91$, $J = -78.6$ cm^{-1}, and $p =$

(24) (a) Riley, P. E.; Davis, R. E.; Allison, N. T.; Jones, W. M. *Inorg. Chem.* **1982**, *21*, 1321. (b) Bauer, D.; Harter, P.; Herdtweck, E. *J. Chem. Soc., Chem. Commun.* **1991**, 829.

(25) (a) Klose, A.; Solari, E.; Re, N.; Floriani, C.; Chiesi-Villa, A.; Rizzoli, C. *Chem. Commun.* **1997**, 2297. (b) Klose, A.; Solari, E.; Floriani, C.; Geremia, S.; Randaccio, L. *Angew. Chem.* **1998**, *110*, 155. (c) Klose, A.; Solari, E.; Hesschenbrouck, J.; Floriani, C.; Re, N.; Geremia, S.; Randaccio, L. *Organometallics* **1998**, *18*, 360.

(26) (a) O'Connor, C. J. *Prog. Inorg. Chem.* **1982**, *29*, 203. (b) Kahn, O. *Molecular Magnetism*; VCH: Weinheim, Germany, 1993.

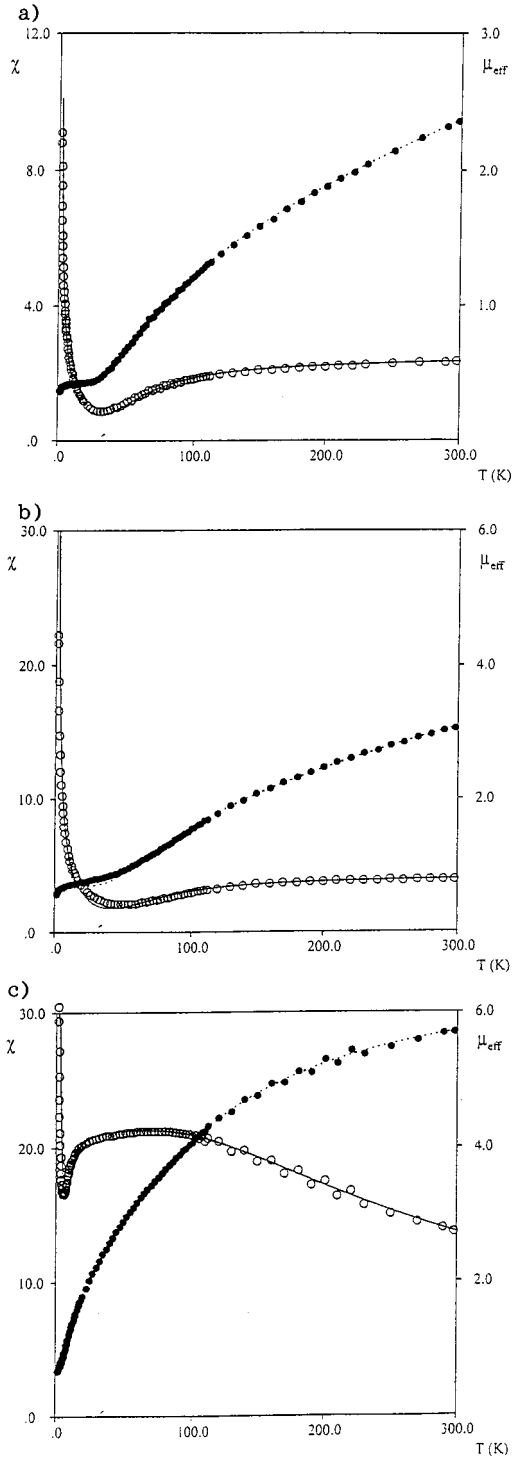

Figure 9. Magnetic susceptibilities (○) and magnetic moments (●) as a function of the temperature for **11** (a), **13** (b), and **14** (c).

0.5% for **11**; $g = 1.94$, $J = -64.1$ cm^{-1}, and $p = 0.6\%$ for **13**; and $g = 2.07$, $J = -9.8$ cm^{-1}, and $p = 1.9\%$ for **14**.

It is noted that the μ-oxo Fe(III)−Fe(III) dimer **11** shows strong antiferromagnetic coupling with a value of J (−78.6 cm^{-1}) in the range reported for several other μ-oxo Fe(III)−Fe(III) dimers.[27] A much smaller antiferromagnetic coupling ($J = -9.8$ cm^{-1}) is instead observed for **14** in the range found for other phenoxo alkoxo or hydroxo-bridged Fe(III) dimers.[28]

(27) Gorun, S. M.; Lippard, S. J. *Inorg. Chem.* **1991**, *30*, 1625 and references therein.

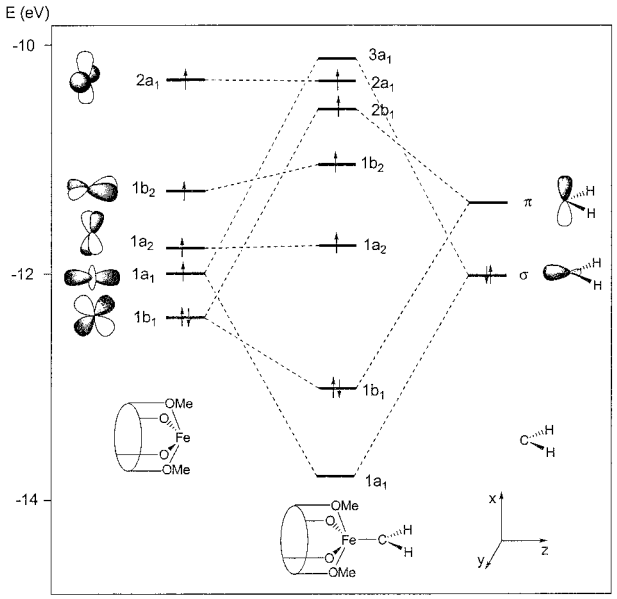

Figure 10. Orbital interaction diagram for complex **17**.

(E) Theoretical Calculations. Extended Hückel calculations[29] were performed on the [{*p*-Bu^t−calix[4]−(O)$_2$(OMe)$_2$}-Fe] fragment, simplifying the calix[4]arene ligand with two phenoxo and two anisoles placed in a C_{2v} geometry. This simplified model retains the main features of the whole ligand; in particular, the geometrical constraints on the O_4 set of donor atoms have been maintained by fixing the geometry of the phenoxo and anisole molecules to the experimental X-ray values.

The frontier orbitals of the [{*p*-Bu^t−calix[4]−(O)$_2$(OMe)$_2$}-Fe] fragment are reported on the left of Figure 10 and consist of four low-lying metal-based orbitals. We can distinguish three lower lying orbitals, i.e., the $1b_1(d_{xz})$, pointing in the plane containing the methylated oxygen, the $1a_1(d_{z^2})$, and the $1a_2(d_{xy})$. Because of the stronger interaction with two phenoxo ligands in the *yz* plane, the $1b_2(d_{yz})$ is almost 1 eV higher in energy than the other d_π orbital, $1b_1(d_{xz})$. The $2a_1(d_{x^2y^2})$ orbital pointing toward the four oxygen ligands is still higher in energy. However, its energy strongly depends on the iron to oxygen distances involving the substituted O(2) and O(4) atoms, which are quite sensitive to the nature of the substituent R and vary from 2.23 Å for R═CH$_3$ in **17** to 2.32 Å for R═Si(CH$_3$)$_3$ in **19A**. In particular, the $2a_1(d_{x^2y^2})$ orbital shows strong decreases in energy on lengthening the above iron to oxygen distances such that it is higher than the $1b_2(d_{yz})$ by almost 1 eV in **17** but by less than 0.4 eV in **19**.

Next, we consider the simplest carbene complex [{*p*-Bu^t−calix[4]−(O)$_2$(OMe)$_2$}Fe═CH$_2$] as a model of the diphenylcarbenes **17**−**19**. The bonding between two moieties is displayed by the interaction orbital diagram in Figure 10. On the extreme right of Figure 10 the frontier orbitals of CH_2, i.e., the σ-donor a_1 (sp^2 hybrid) and the p-acceptor $b_2(p_y)$, are presented. Because of the quintet spin state of for this complex, the bonding between the metal fragment and the CH_2 unit, illustrated in the second column of Figure 10, is quite different from that arising from the usual molecular orbital interpretation of carbene complexes.[30] Two main interactions are still observed between the σ-donor

(28) Snyder, B. S.; Patterson, G. S.; Abrahamson, A. J.; Holm, R. H. *J. Am. Chem. Soc.* **1989**, *111*, 5214 and references therein.
(29) (a) Hoffmann, R.; Lipscomb, W. N. *J. Chem. Phys.* **1962**, *36*, 2179. (b) Hoffmann, R. *J. Chem. Phys.* **1963**, *39*, 1397.
(30) Hoffmann, P. In *Transition Metal Carbene Complexes*; Verlag Chemie: Weinheim, Germany, 1983; p 113.

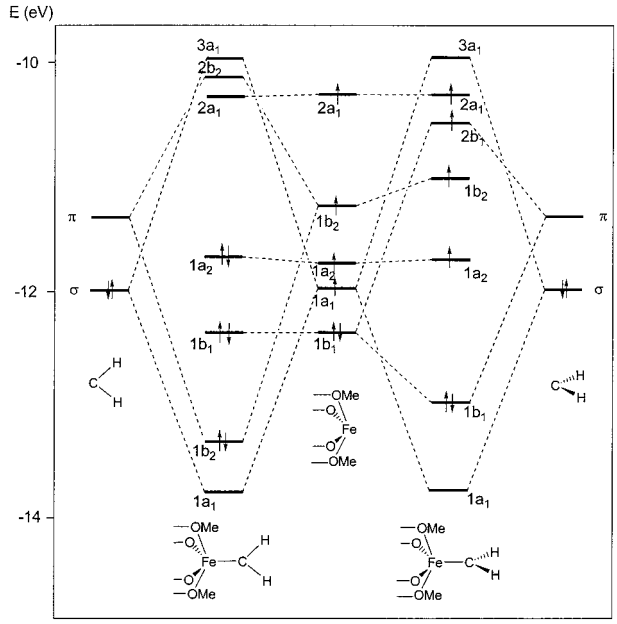

Figure 11. Orbital interaction diagram of two conformations.

orbital a_1 of CH_2 and the σ-acceptor metal orbital $1a_1(d_{z^2})$, and between the π-acceptor b_2 of CH_2 and the π-donor $1b_1(d_{xz})$. However, one of the four unpaired electrons occupies the π^* metal−carbene antibonding orbital, thus reducing the metal−carbon bond order. This is in agreement with the experimental evidence showing long Fe−C bond distances (1.943 Å in **17**, 1.958 Å in **19A**, and 1.973 Å in **19B**), which are closer to a single bond than to a double bond. This arrangement is probably favored by the particular orientation imposed by the steric hindrance between the carbene phenyl rings and the methyl or trimethylsilyl groups on the O(2) and O(4) oxygens. Indeed, for both complexes **17** and **19**, the X-ray structures show that the carbene plane lies essentially in the *xz* symmetry plane passing through Fe, O(1), and O(3), the orientation relieving the above steric interaction. However, this is not the preferred carbene orientation expected on the basis of frontier orbital patterns of the metal fragment.

In principle the π-acceptor orbital of CH_2 can interact with either the $1b_2(d_{yz})$ or $1b_1(d_{xz})$ metal orbitals, leading to different orientations of the carbene moiety with the CH_2 unit lying in the *xz* or *yz* plane, i.e., the Fe−O(2)−O(4) or Fe−O(1)−O(3) plane, respectively. According to the general rules for orbital interactions,[31] the carbene π-acceptor level should preferentially interact with the higher-lying $1b_2(d_{yz})$ so that the preferred carbene orientation is expected to be that in the Fe−O(2)−O(4) plane. This orientation, however, cannot be achieved because of the intraligand steric hindrance, which forces the complex to the experimentally observed orientation with the carbene in the Fe−O(1)−O(3) plane. As a consequence of this sterically imposed orientation, the interaction between the π level of the carbene and the low-lying metal $1b_1(d_{xz})$ is quite weak, leading to a relatively low-energy π^* metal−carbene antibonding orbital, which allows its population to favor the high-spin state. This picture is confirmed by our extended Hückel calculations on the [{*p*-Bu^t−calix[4]−$(O)_2(OMe)_2$}Fe═CH_2] model complex, which cannot have any intraligand steric hindrance. Separate calculations have been performed on the singlet states of the two possible carbene conformations, and that with the carbene in the Fe−O(2)−O(4) plane resulted in a configuration that is ca. 22 kcal/mol more stable than the experimental conformation. Moreover, the molecular orbital diagram for the two conformations reported in Figure 11 illustrates clearly that the hypothetical conformation with the carbene in the Fe−O(2)−O(4) plane shows a stronger metal−carbene p interaction and much higher lying π^*(Fe−C) orbital, which would probably favor a conventional low-spin carbene with the usual iron−carbon double bond character. This arrangement can be described as a sterically driven high-spin state.

(31) Albright, T. A.; Burdett, J. K.; Whangbo, M. H. *Orbital Interaction in Chemistry*; Wiley: New York, 1985.

Conclusions

The reactivity of the iron-bis-O-alkylated calix[4]arene explored in this paper gives significant insight on the redox behavior of iron(II) in a square-planar environment made up of oxygen donor atoms only. The oxidation state (III) seems to be, under the explored conditions, the only accessible one. In the meantime, the parent compound, when reacted with diazoalkanes, led to the formation of Fe═C functionalities in metallacalix[4]arene derivatives. This result revealed how such a functionality, which is a key intermediate in the Fischer−Tropsch synthesis, can be easily bound to an iron−oxo surface.

Acknowledgment. We thank the "Fonds National Suisse de la Recherche Scientifique" (Bern, Switzerland, Grant No. 20-53336.98), Action COST D9 (European Program for Scientific Research, OFES No. C98.008), and Fondation Herbette (University of Lausanne, N. Re) for financial support.

Supporting Information Available: ORTEP drawings, details of the X-ray data collection, structure solution and refinement, and tables giving crystal data, atomic coordinates, isotropic and anisotropic displacement parameters, and bond lengths and angles for **8**, **9**, **12**, **14**, **16**, **17**, **and 19**. This material is available free of charge via the Internet at http://pubs.acs.org.

IC991467H